Journal of Polymer Research (2021) 28: 348
https://doi.org/10.1007/s10965-021-02673-0

ORIGINAL PAPER

Chitosan-capped silver nanoparticles: fabrication, oxidative dissolution, sensing properties, and antimicrobial activity

Zoya Zaheer[1]

Received: 18 February 2021 / Accepted: 12 July 2021 / Published online: 20 August 2021

Abstract

Chitosan-capped stable silver sols (Chit/AgNPs) were fabricated using a chemical reduction method. Chit/AgNPs exhibited a sharp surface plasmon resonance (SPR) peak at 420 nm. The resulting orange-colored sols became colorless after the addition of ferric (Fe^{3+}) ions at room temperature. Chitosan formed a stable complex with Fe^{3+} ions. The relative viscosity measurements revealed that the chitosan was stable in the presence of hydrogen peroxide at room temperature for ca. 1 h. Hydrogen peroxide catalyzed the Fe^{3+} sensing activity of the Chit/AgNPs, and the mechanism proceeded through a Fenton-like reaction. The AgNPs were oxidized by Fe^{3+} ions into silver ions. The Al^{3+}, Ba^{2+}, Ca^{2+}, Cu^{2+}, Co^{2+}, Mg^{2+}, Ni^{2+}, Pb^{2+}, Zn^{2+}, Na^{+}, and K^{+} did not act as sensors for AgNPs. The plasmonic colorimetric detection limit of Fe^{3+} ions was found to decrease (from 20 to 100 µM) with the pH of the working solution. The microbial growth of chitosan and Chit/AgNPs was evaluated against *S. aureus* and *C. albicans* human pathogens using optical density measurements. Chitosan prevented electrolyte exchange on the surface of the bacterial cell walls and disturbed the cells' physiological functions.

Keywords Silver sensor · Chitosan · Coordination · Ferric ions · Detection

Introduction

Synthesis and characterization of coated plasmonic nanoparticles (NPs) with polymers such as proteins [1], chitosan [2], gelatin [3], gum acacia [4], carbohydrates [5], polyvinyl alcohol [6], polyvinylpyrrolidone [7], polymer hydrogels [8, 9], starch [10], and other polymers [11, 12] have garnered interest among a number of investigators due to their potential application in medicine and industry. Water-soluble silver and gold NPs have been fabricated using chitosan as capping agent for various applications. Shen and coworkers prepared chitosan-ferric ion hydrogel for the adsorption and desorption of various toxic dyes [13]. Zimmermann et al. used chitosan-ferric cross-linked complex as an adsorbent to the removal of chromium (VI) from wastewater [14]. A chitosan-copper-ferric bimetal complex was synthesized by a precipitation method and used for the catalytic degradation of toxic dyes in the presence of hydrogen peroxide [15]. Begum and coworkers used various polymer microgels for the stabilization AgNPs by the sol–gel method. The as-prepared AgNPs were used as a catalyst for the reduction of nitroarenes in aqueous medium [16–18]. Farooqi et al. reported the catalytic degradation of malachite green using a cross-linked colloidal microgel system loaded with AgNPs [19]. El-Sherbiny et al. prepared hyper-branched chitosan-capped AgNPs for the detection of ammonia [20]. Sugunan et al. prepared chitosan-capped AuNPs using glutamate as a reducing agent for the detection of copper and zinc ions in water [21]. Thiol-chitosan AgNPs showed excellent sensitivity toward Hg^{2+} ions in water [22]. Jiang and coworkers used chitosan-capped AgNPs for the colorimetric estimation of glucose [23]. The literature contains abundant reports on the synthesis of silver and gold NPs in the presence of different capping agents and their application as sensing agents for the detection of heavy toxic metal ions and for visual detection of organic molecules (acetaldehyde, glucose, aromatic phenols, and toxic dyes) [24–30]. Naseem et al. used polymer microgel particles and AgNPs stabilized with microgel as an adsorbent and catalyst for the removal of toxic dyes, heavy metals, and aryl nitro compounds from aqueous media, respectively [31–33].

Iron is an essential element for human and animal bodies and governs the transport of oxygen via metal complexes during the oxygenation of blood. Ferric ions were found to form

✉ Zoya Zaheer
zoya.zaheer@gmail.com

[1] Department of Chemistry, Faculty of Science, King Abdulaziz University, P. O. Box 80203, Jeddah 21589, Saudi Arabia

stable complexes with chitosan in acidic pH [34]. Cobley and coworkers reported the controlled etching of silver from the surface of polyvinylpyrrolidone-capped Ag nanocubes by adding ferric ions, $K_3Fe(CN)_6$, and $K_4Fe(CN)_6$) in an aqueous solution [35]. Guo et al. used ferric ions as an oxidative etching agent for the removal of AgNPs from core–shell Au@Ag nanorods with and without hydrogen peroxide in the presence of CTAB [36]. Fenton (a solution of ferrous/ferric and hydrogen peroxide) and Fenton-like reactions generated reactive oxygen species [37], which were responsible for the degradation of water contaminants, oxidation of organic compounds, and dissolution of plasmonic AgNPs in the presence of hydrogen peroxide. Wang developed a colorimetric sensing method for the detection of iodide using AgNPs and hydrogen peroxide [38]. AgNPs stabilized with starch [39], graphene [40], gum polysaccharide [41], and gelatin [42] were used as a surface plasmon resonance (SPR)-based sensor for the detection of hydrogen peroxide. The oxidation kinetics of AgNPs has attracted the interest of various researchers. Khan and coworkers reported the kinetics of oxidative dissolution of starch and CTAB-capped AgNPs with varying experimental conditions [10, 43]. The application of AgNPs as sensors for the detection of heavy metal ions and removal of dye has been studied extensively, but no studies have investigated the etching of silver from the surface of chitosan-capped AgNPs by Fenton-like reaction. Therefore, systematic information is needed to establish the optical sensing etching mechanism of AgNPs through reactive oxygen species. Chitosan is an excellent biocompatible, nontoxic, and biodegradable stabilizing agent for metal NPs. It can coordinate with metal ions and/or NPs through amino and hydroxyl groups.

In the present study, chitosan was chosen as complexing and stabilizing agent for the synthesis of AgNPs, which were used as a selective optical sensor (visual color change from orange to colorless) for the detection of Fe^{3+} ions. We investigated, for the first time, the Fenton-like oxidative etching of silver ions from chitosan-capped AgNPs using Fe^{3+} ions and hydrogen peroxide. We observed that the SPR intensity of AgNPs decreased with increasing concentrations of Fe^{3+}, and hydrogen peroxide.

Experimental

Materials

Medium-molecular-weight chitosan, glacial acetic acid (CH_3COOH, ≥ 99.7%), sodium borohydride ($NaBH_4$, 99%), silver nitrate ($AgNO_3$, ≥ 99.7%), sodium hydroxide (NaOH, ≥ 98%), sodium acetate (CH_3COONa, ≥ 99%), hydrogen peroxide (30% w/w in water), 1,10-phenanthroline ($C_{12}H_8N_2$, ≥ 98%), inorganic salts of 99% purity ($NaNO_3$, KNO_3, $Ba(NO_3)_2$, $Ca(NO_3)_2$, $Cu(NO_3)_2$, $Co(NO_3)_2$, $Mg(NO_3)_2$, $Ni(NO_3)_2$, $Pb(NO_3)_2$, $Zn(NO_3)_2$, $Fe(NO_3)_3$, and $Al(NO_3)_3$) and scavengers (methanol, n-butanol, KI, and t-butanol) were purchased from Sigma-Aldrich. Deionized and double-distilled water was used as solvent throughout all measurements. The solutions of all metal ions (0.001 mol/L) were prepared in water on a molar basis. The $AgNO_3$ solution (0.01 mol/L) was stored in a brown glass bottle and kept in the dark to prevent the photochemical degradation of Ag^+ ions. $NaBH_4$ solution was prepared daily before the experiments. The glassware was washed with 5% HNO_3 and dried prior to use.

Chitosan solution and determination of viscosity average molecular weight

Chitosan solution (2% w/v) was prepared in acetic acid (1.0% v/v) with constant stirring at 60 °C for 24 h to obtain a clear solution. The intrinsic viscosity was measured in a solution of acetic acid (0.1 M) and NaCl (0.2 M) with an Ubbelohde capillary viscometer [44]. The M_w was calculated using the Mark–Houwink–Sakurada relation (Eq. 1):

$$[\eta] = K(M_w)^a \quad (1)$$

where $[\eta]$ = intrinsic viscosity of chitosan solution. The parameters ($K = 3.5 \times 10^{-4}$) and ($a = 0.96$) are the empirical constants, which depend on the experimental conditions [45]. The M_w was found to be 370 kD.

Chitosan-capped AgNP synthesis and characterization

For the preparation of chitosan-capped AgNPs, the Ag^+ solution (2.0 mM) was mixed in a stoppered 250 ml conical flask containing 5 ml of chitosan solution as prepared in acetic acid, and distilled water (20 ml for dilution) at a fixed pH (= 5.0). The resulting solution was stirred at room temperature for 1 h to ensure coordination of Ag^+ with the $–NH_2$ group of chitosan. The aqueous solution of $NaBH_4$ (3.0 mM) was rapidly added to the reaction vessel (total volume = 50 ml). The colorless chitosan-Ag^+ solution became yellow to red–orange as the reaction time increased. The resulting red–orange-colored chitosan-Ag nano-sols were stable for ca. 2 months and stored in a refrigerator. A UV–visible spectrophotometer (Shimadzu UV-260) was used to monitor the optical properties of the Chit/AgNPs. A transmission electron microscope (TEM, JEOL JEM-1400) equipped with an energy-dispersive X-ray detector (EDX) operating at a beam energy of 100 keV was used to determine the morphology (size, shape, and size distribution) of the Chit/AgNPs. For TEM measurements, samples were prepared by adding droplets of resulting silver sols onto

copper–carbon-coated grids (300 mesh) and allowing them to dry at room temperature in a dry box.

A ninhydrin color test was performed to detect the presence of chitosan on the surface of the as-prepared chitosan-AgNPs. For the formation of blue color (Ruhemann's purple), ninhydrin reagent was prepared in acetic acid–sodium acetate buffer at pH 5.5. The required amount of reagent was added into the silver sols and heated for 5 min in a boiling water bath. The appearance of purple color indicated the presence of chitosan on the surface of AgNPs (Eq. 2).

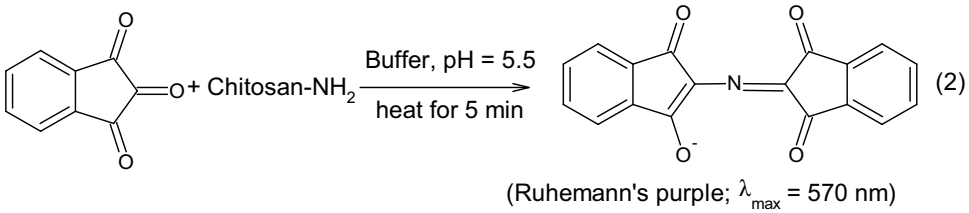

(Ruhemann's purple; λ_{max} = 570 nm) (2)

Optical detection of metal ions in water

In order to determine the limit of detection of metal ions, a series of experiments were performed separately for Al^{3+}, Fe^{3+}, Ba^{2+}, Ca^{2+}, Cu^{2+}, Co^{2+}, Mg^{2+}, Ni^{2+}, Pb^{2+}, Zn^{2+}, Na^{+}, and K^{+} by adding the same amount of metal ions (5 ml of 0.001 mol/L) in different reaction flasks containing 10 ml of as-prepared chitosan-capped silver sols. The progress of the reaction was observed by visual color change. The orange color of chitosan-AgNPs became colorless within ca. 10 min only for the Fe^{3+} reaction flask. UV–visible spectra and photographs were recorded. The effects of Fe^{3+} ion concentration (from 20 to 100 µM) on the decay in SPR intensity was investigated at a fixed concentration of chitosan-AgNPs, and the limit of detection was calculated using Eq. (3) (*vide infra*).

$$Limit\ of\ \det ection = \frac{3\sigma}{Slope\ of\ calibration\ curve} \quad (3)$$

To detect the in situ formation of Fe^{2+} ions during the etching of Ag^{+} ions from the surface of chitosan-AgNPs by Fe^{3+} ions, 1,10-phenanthroline was added to the reaction mixture, and absorbance of a red color complex ($[Fe(phenanthroline)_3]^{2+}$) was recorded at 510 nm.

Optical sensing with Fenton-like reagent

The optical sensing of Fe^{3+} ions by chitosan–AgNPs was performed in the presence of H_2O_2. In a typical experiment, different concentrations of H_2O_2 (from 0.1^4 to 0.40 mM) were added in to the reaction flask containing the required amount of chitosan-AgNPs and Fe^{3+} ions. The decreases in SPR intensity at 420 nm were monitored as a function of time. The reactive oxygen species ($^{\cdot}OH$ and $O_2^{\cdot -}$) were generated during the oxidative dissolution of AgNPs with H_2O_2. The same kinetic experiments were performed in the presence of scavengers to establish the role of $^{\cdot}OH$ and $O_2^{\cdot -}$.

Microbial growth kinetics

The optical density (OD) method was used to determine the growth kinetics of human pathogens against chitosan and Chit/AgNPs. Luria–Bertani (LB) broth was used as a source for the preparation of bacterial cultures at 37 °C. The required amount of bacterial culture and chitosan was mixed, and optical density was measured at a wavelength of 600 nm and temperature of 37 °C, with constant time intervals. The optical density was maintained from 0.1 to 1.0 for ideal cell concentration (OD of 0.1 = concentration of 10^8 cells/ml) [46]. The AgNP concentration was varied from 10 µM to 40 µM in LB culture media. The control and reference experiments were performed without AgNPs and bacteria, respectively, in the same LB. The growth rate constants were evaluated by a conventional technique (from the slope of lnOD versus time plots with a fixed time method). The same experiments were repeated for only chitosan solution.

Results and discussion

Chitosan-capped AgNP sensing with Fe^{3+}

Chitosan was used as a stabilizing and/or coordinating agent for the fabrication of AgNPs in the presence of $NaBH_4$ (strong reducing agent). The UV–visible spectrum of AgNPs showed a SPR peak only at ca. 420 nm (Fig. 1A). Mie's theory predicts only a single SPR band in the absorption spectra of spherical nanoparticles. On the other hand, anisotropic particles could give rise to two or more SPR bands depending on the shape [47]. Sun and Xia reported that the number of SPR bands increased with decreasing symmetry of the nanoparticles [48]. The prominent single peak at 420 nm is consistent with the spherical nature of the AgNPs [49, 50]. The number of silver atoms per nanoparticle (*N*) and molar concentration (C) of AgNPs were calculated using Eqs. (4) and (5) [51].

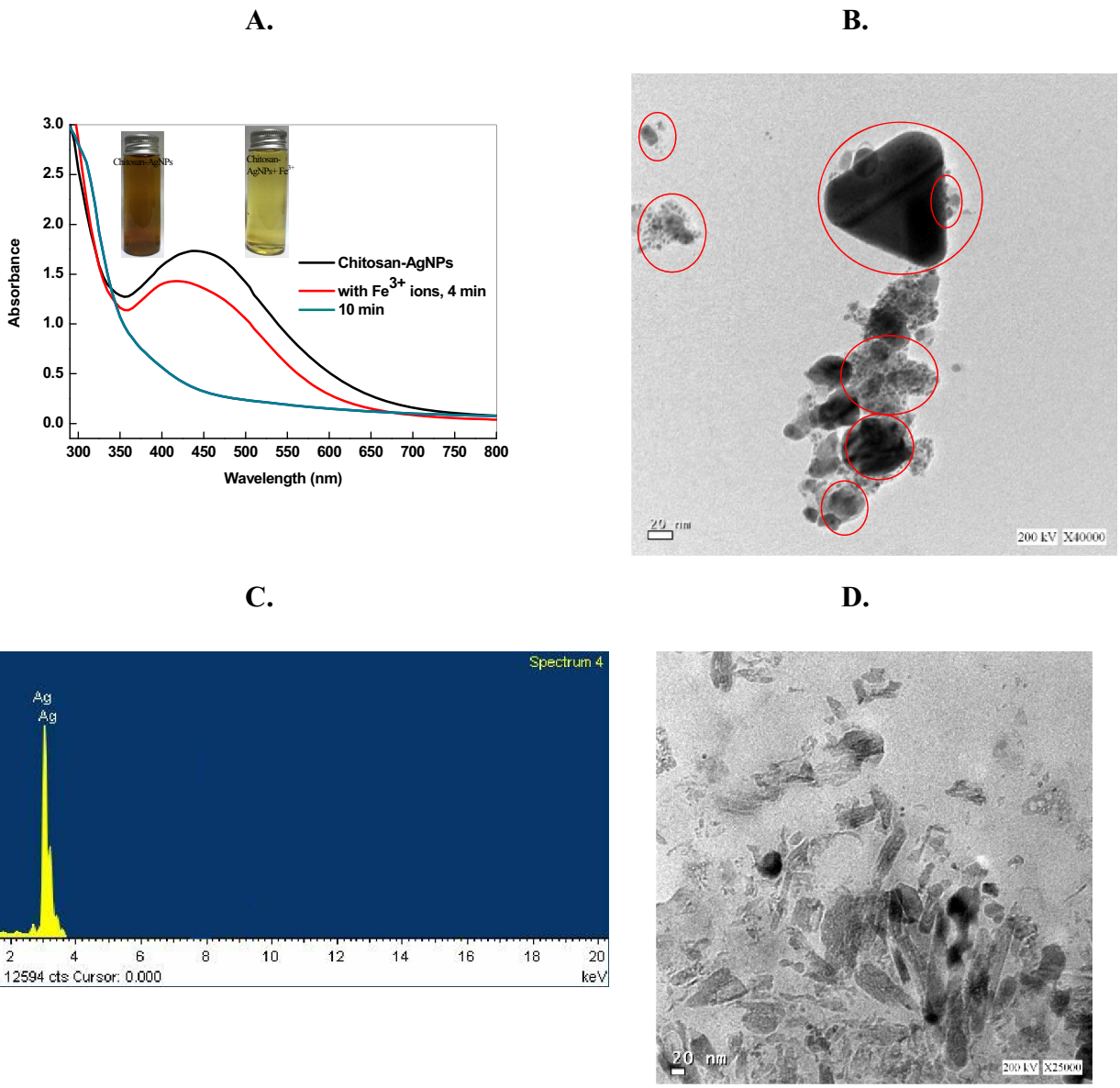

Fig. 1 UV–visible spectra of pure Chit/Ag and Chit/Ag + Fe^{3+} as a function of time (**A**), TEM image (**B**), EDX (**C**), and TEM image after complete dissolution of AgNPs (**D**). Inset: optical images of Chit/Ag and oxidized AgNPs. Reaction conditions: [AgNPs] = 10.0×10^{-4} M, [Fe^{3+}] = 100 µM, and pH = 5.0

$$N = \frac{3.14 \times \rho \times 6.02 \times 10^{23}}{6 \times M} \times D^3 \tag{4}$$

$$C = \frac{N_T}{N \times V \times 6.02 \times 10^{23}} \tag{5}$$

where ρ, M, D, N_T, and V are the density of face-centered cubic silver, atomic mass of silver, average diameter of AgNPs calculated by TEM analysis, total number of silver atoms added as metal salt precursor, and volume of the reaction mixture, respectively. The value of N was estimated ($= 1.8 \times 10^5$) with Eq. (18) by substituting all the parameters. For the molar concentration, the values of N_T ($= 0.1$), N ($= 1.8 \times 10^5$), and V ($= 0.02$) were substituted into Eq. (5), and C was found to be 2.7×10^{-5} mol/L.

The TEM images show that the AgNPs are mostly nanospheres. Inspection of TEM images clearly indicates that the nanospheres are aggregated in an asymmetrical manner, leading to the formation of spherical (size ranging from ca. 4 to 40 nm), triangular, and irregular-shaped NPs as indicated by red circles (Fig. 1B). The aggregation of nanospheres might be due to the presence of a large number of different

functional groups ($–NH_2$ and –OH) in the backbone of the chitosan polymer. A thin black layer of other organic material was also visualized on the surface of NPs, indicating the capping action of chitosan [52, 53]. EDX images show that the as-prepared sample had 100% metallic silver (Fig. 1C). The optical images also showed that the resulting silver sols were stable for ca. 2 months without any visually apparent aggregation or precipitation. The Fourier transform infrared spectrum of chitosan shows the main characteristic bands at 3420 to 3120 cm^{-1} for the –OH and $–NH_2$ group stretching vibrations, 1735 cm^{-1} for $–NH_2$ bending vibrations, 1110 cm^{-1} for C–O stretching polysaccharide, and 880 cm^{-1} for the 1,4-glycosidic bond. For Chit/Ag, these bands are shifted slightly from 3420 to 3390, 3120 to 3110, and 1735 to 1720 cm^{-1}, and the band intensity is also decreased, indicating the coordination of metallic silver with the $–NH_2$ and –OH groups of chitosan [54]. The ninhydrin color test was performed to establish the capping role of chitosan. Ninhydrin produces a characteristic purple color with a free $–NH_2$ group. The as-prepared silver sol was treated with ninhydrin solution (2.0 mM, prepared in acetic acid–sodium acetate buffer of pH 5.0) and heated at 80 °C for 5 min. The absorbance of the purple color was monitored at 570 nm with varying concentrations of Chit/AgNPs. The appearance of the purple color indicated the presence of chitosan on the surface of the AgNPs [55, 56].

To investigate the sensing properties of Chit/Ag, a series of experiments were performed by adding different amounts of Fe^{3+} ion aqueous solution in a Chit/Ag sol. In a typical experiment, Fe^{3+} ions (from 20 to 100 µM) were used to determine the sensing properties of 10 ml of Chit/AgNP colloidal solution. Visual observations indicated that the AgNPs reacted very quickly with Fe^{3+}, and a dramatic color change from orange to colorless was found. Figure 1A also shows the effect of Fe^{3+} on the color change of Chit/Ag NPs. To determine the quantitative sensing role of Fe^{3+}, UV–visible spectra of Chit/Ag were recorded with different concentrations of Fe^{3+} at definite time intervals. Figure 2 (grey line) shows that the pure chitosan absorbs at ca. 210 nm in the ultraviolet region (with no color). For Fe^{3+} ions, one peak and a shoulder appeared at 220 and 300 nm, respectively, in water due to the charge transfer bands (Fig. 2; red line). Chit/Ag exhibited a sharp SPR band in the visible region at 420 nm for AgNPs and another band at ca. 240 nm for the coordinated chitosan. Interestingly, the SPR intensity of AgNPs changed very rapidly with increasing concentrations of Fe^{3+} ions, and the orange color became colorless at higher Fe^{3+} (≥ 100 µM). A small concentration (= 20 µM) was enough to decrease the SPR intensity of AgNPs from 1.22 to 1.01 (17.2% decrease in SPR). Thus, Chit/Ag acted as an excellent nanosensor for Fe^{3+}. The TEM image of Chi/AgNPs was also measured after 10 min of sensing reaction time. The morphology of NPs

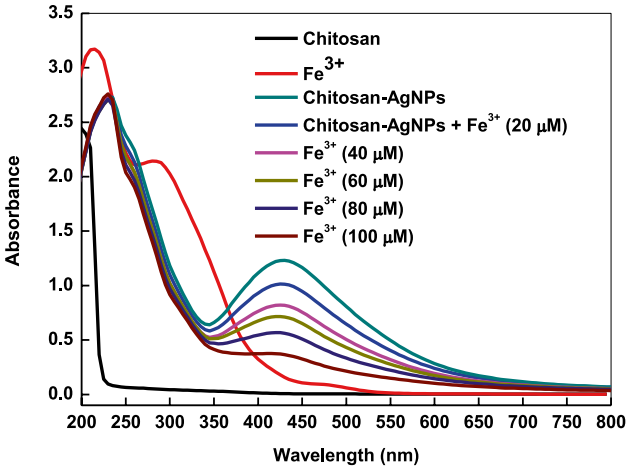

Fig. 2 UV–visible spectra of pure chitosan, Fe^{3+} and Chit/Ag and Chit/Ag + Fe^{3+} as a function of concentration. Reaction conditions: [AgNPs] = 8.0×10^{-4} M, and pH = 5.0

was completely changed from spherical–triangular to undefined polydisperse NPs (Fig. 1D), indicating the dissolution of AgNPs with Fe^{3+} ions.

In order to determine the limit of detection, a calibration curve was constructed between the change in absorbance ($A_0 - A$; where A_0 and A are the absorbance of Chit/Ag in the absence and presence of Fe^{3+} ions, respectively) and [Fe^{3+}]. It was observed that the value of $A_0 - A$ increased with increasing concentration of Fe^{3+}, and a linear correlation was found with the slope (= 0.00748) and linear regression coefficient ($R^2 = 0.995$) for the entire concentration range used in the present study (Fig. 3A). Equation (3) was used to calculate the limit of detection for Chit/Ag for the analysis of Fe^{3+} for three times the standard deviation, which was found to be 7.33×10^{-8} M (= 73.3 nM) under our experimental conditions. The decay in SPR intensity was also monitored as a function of time for various [Fe^{3+}]. The reaction–time profile shows that the complete dissolution of SPR intensity was observed within 10 min at higher Fe^{3+} concentration (Fig. 3B) at pH 5.0. The oxidative dissolution rate constants (k_{obs}) were calculated from the first-order rate equation ($k_{obs} = 2.303/t \log (A_\alpha - A_0/A_\alpha - A_t)$. It was found that the plots of log(Absorbance) versus time were linear, and k_{obs} (3.1, 4.7, 6.7, 7.0 and 7.6×10^{-3} s^{-1} for [Fe^{3+}] = 20, 40, 60, 80, and 100 µM, respectively) was estimated from the slope of these plots (Figure S1, supporting information). The plot of k_{obs} versus Fe^{3+} concentration was nonlinear (Figure S2; concave curve). The double-reciprocal plot between k_{obs} and Fe^{3+} concentration was linear, with a positive intercept on the *y*-axis, suggesting complex formation between AgNPs and Fe^{3+} prior to electron transfer. The pH effect was also studied (ranging from 2.0 to 5.5) at fixed concentrations of Chit/AgNPs (= 10.0×10^{-4} mol/L) and

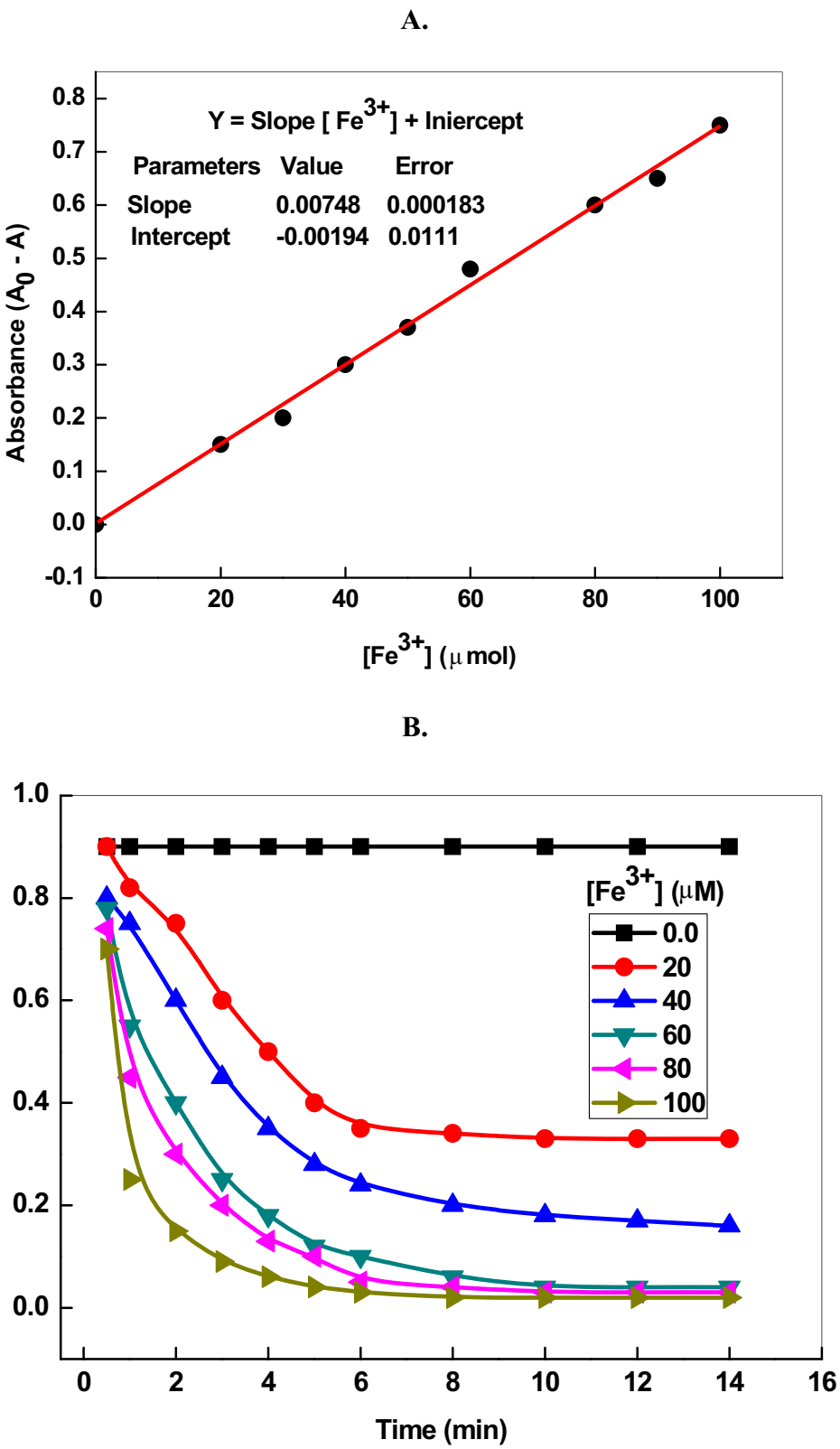

Fig. 3 Plot of absorbance intensity ($A_0 - A$) versus Fe^{3+} concentration (**A**) and reaction–time profiles for the dissolution of AgNPs by Fe^{3+} **B** Reaction conditions: [AgNPs] = 8.0×10^{-4} M, and pH = 5.0

Fe^{3+} (= 40 μM). The k_{obs} values were found to increase with increasing pH ($10^3 k_{obs}$ = 0.3, 1.6, 2.6, 4.7, and 5.2 s^{-1} for pH 2.0, 3.5, 4.5, 5.0, and 5.5, respectively). The reaction mixture became turbid at higher pH (≥ 6.0), and a red-brown gelatinous mass was formed. Therefore, studies were limited to the acidic pH range.

Mechanism of AgNP sensing

The standard reduction potentials of Ag^+/Ag^0 and Fe^{3+}/Fe^0 are responsible for the sensing of AgNPs for the detection of Fe^{3+}. The potentials of these redox couples are as follows [Eqs. (6) to (8)].

$$Ag^{+}_{aq} + e^{-} \rightarrow Ag^{0}_{s} \qquad (+0.80V) \tag{6}$$

$$Fe^{3+}_{aq} + e^{-} \rightarrow Fe^{2+}_{aq} \qquad (+0.77V) \tag{7}$$

$$Fe^{2+}_{aq} + 2e^{-} \rightarrow Fe^{0}_{s} \qquad (-0.44V) \tag{8}$$

The etching of Ag shell from core–shell Au-AgNPs by Fe^{3+} has been reported, and the redox reaction between AgNPs and Fe^{3+} was found to be responsible for the decrease in the SPR intensity of the AgNPs [35]. The Fe^{3+} ions formed a complex with water due to their tendency to hydrolyze and/or to form complexes and exist as $Fe(H_2O)_6{}^{3+}$. The hydroxo species, $([Fe(OH)(H_2O)_5]^{2+}$, are formed in acidic media (PH ≤ 4.0) due to the first stage of acid dissociation of the aqua ion [57]. The $[Fe(OH)(H_2O)_5]^{2+}$ are yellow in color due to charge transfer bands in the ultraviolet region. The $[Fe(OH)(H_2O)_5]^{2+}$ is the major reactive species of Fe^{3+} aqua ion at pH ≤ 5.0. The presence of –OH species will facilitate the complex formation between AgNPs and Fe^{3+} [43]. The mechanism in Scheme 1 is proposed for the oxidative dissolution of AgNPs.

$$Fe(H_2O)_6{}^{3+} \overset{K_h}{\rightleftharpoons} \left[Fe(OH)\left(H_2O\right)_5\right]^{2+} + H^{+} \tag{9}$$

In Scheme 1, Eq. (9) represents the hydrolysis of Fe^{3+} ions into $[Fe(OH)(H_2O)_5]^{2+}$, which is the reactive species of the aqua ion. Chit/Ag formed a complex with $[Fe(OH)(H_2O)_5]^{2+}$ (Eq. 10), which would undergo a unimolecular one-step oxidation–reduction in the next step (Eq. 11) due to the higher reduction potential of Ag^+/Ag^0 to Fe^{3+}/Fe^0. Finally, orange-colored silver sol became colorless within 20 min of reaction time. To detect the formation of Fe^{2+}, 1,10-phenanthroline was also added to the colorless reaction mixture, and a red color immediately appeared, which indicated the reduction of Fe^{3+} ions into Fe^{2+} by metallic silver. The oxidation and reduction of AgNPs and Fe^{3+}, respectively, took place simultaneously. Chitosan formed a complex with the in situ generation of Fe^{2+} ions (Fig. 2; brown line). Ammonium chloride and hydroxide were also added to the reaction mixture after the complete SPR dissolution of AgNPs. No brown precipitate of $Fe(OH)_3$ appeared, ruling out the presence of Fe^{3+} in the resulting solution. Thus, AgNPs and Fe^{3+} were completely oxidized and reduced into Ag^+ and Fe^{2+}, respectively, under the experimental conditions.

The following rate laws [Eqs. (12) and (13)] were derived from the Scheme 1 mechanism.

$$-\frac{d[AgNPs]}{dt} = \frac{kK_cK_h[Fe^{3+}][Chit/Ag]_T}{[H^+] + K_cK_h[Fe^{3+}]} \tag{12}$$

$$k_{obs} = \frac{kK_cK_h[Fe^{3+}]}{[H^+] + K_cK_h[Fe^{3+}]} \tag{13}$$

The reverse of Eq. (13) can be written as Eq. (14) to further analyze the data.

$$[Fe(OH)(H_2O)_5]^{2+} + \text{Chit-}(Ag^0)_n \overset{K_c}{\rightleftharpoons} \text{Chit-}(Ag^0)_{n-1}\text{-}Ag^0\text{-}[Fe(OH)(H_2O)_5]^{2+} \tag{10}$$

(λ_{max} = 420 nm) (complex)

$$\text{Complex} \xrightarrow{k} \text{Chitosan} - Fe^{2+} + nAg^{+} + 5H_2O + OH^{-} \tag{11}$$

$$1/k_{obs} = \frac{[H^+]}{kK_cK_h[Fe^{3+}]} + \frac{1}{k} \tag{14}$$

Scheme 1 Sensing of Chit/AgNPs with Fe^{3+}

$$Fe(H_2O)_6{}^{3+} \overset{K_h}{\rightleftharpoons} [Fe(OH)(H_2O)_5]^{2+} + H^{+}$$

$$[Fe(OH)(H_2O)_5]^{2+} + \text{Chit-}(Ag^0)_n \overset{K_c}{\rightleftharpoons} \text{Chit-}(Ag^0)_{n-1}\text{-}Ag^0\text{-}[Fe(OH)(H_2O)_5]^{2+}$$

(λ_{max} = 420 nm) (complex)

$$\xrightarrow{k} \text{Chitosan-}Fe^{2+} + nAg^{+} + 5H_2O + OH^{-}$$

According to Eq. (14), the plot of 1/kobs versus 1/[Fe3+] should be linear (Figure S3). The values of k (= 0.0119 s^{-1}) and Kc Kh (= 0.179) were calculated from the intercept and slope of Figure S3. The close agreement between the experimental and calculated rate constant (Table 1) provides the supporting evidence to the proposed mechanism.

Role of chitosan in Fe^{3+} sensing

To establish the role of free chitosan on the oxidative dissolution of Chit/AgNPs with Fe^{3+}, a different amount of chitosan (0.2% of 2 ml to 8 ml) was added in different reaction flasks containing Chit/AgNPs + Fe^{3+}. Figure 4 shows that the chitosan inhibited the Fe^{3+}-catalyzed dissolution of AgNPs. Chitosan is soluble and insoluble in acidic and alkaline medium due to the protonation and deprotonation of pH-sensitive $–NH_2$ groups, respectively. It has a strong tendency to coordinate with metal ions. Henglein suggested that the Ag^0 forms a complex with Ag^+ ($Ag^0 + Ag^+ \leftrightarrow Ag_2^+$), which undergoes fast dimerization ($Ag_2^+ + Ag_2^+ \leftrightarrow Ag_4^{2+}$), and the resulting species of AgNPs bears positive charges [58]. The stability constant of chitosan-Fe^{3+} (logβ = 16.06) was higher than that of the Ag^+-NH_3 complex (logβ = 7.2). Therefore, Fe^{3+} ions have a strong tendency to form a complex with the –OH and $–NH_2$ groups of chitosan. In a reaction mixture (Chit/AgNPs + Fe^{3+} + chitosan), competition exists between chitosan and AgNPs to react with Fe^{3+}. The Fe^{3+} does not exist as aqua free ions. The reduction potential of metal ions is decreased to some extent after complex formation with a suitable ligand [59]. Coordination of chitosan with Fe^{3+} reduced the electron-gaining tendency of Fe^{3+} to some extent, and Chit/Ag + Fe^{3+} + chitosan became more complicated. The inhibitory effect of chitosan can be attributed to the complex formation between free chitosan and Fe^{3+}.

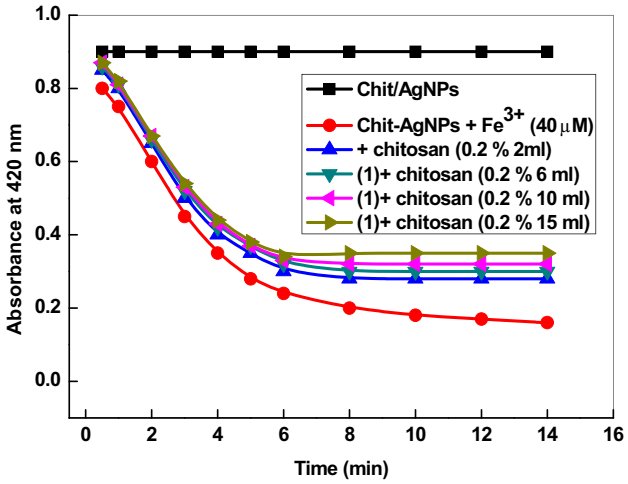

Fig. 4 Reaction–time profiles for the dissolution of AgNPs by Fe^{3+} as a function of chitosan concentration. Reaction conditions: [AgNPs] = 8.0×10^{-4} M, [Fe^{3+}] = 40 μM, and pH = 5.0

Effects of H_2O_2 on Fe^{3+} sensing

To investigates the influence of H_2O_2 on the Fe^{3+}-assisted dissolution of Chit/AgNPs, different amounts of H_2O_2 (from 0.10 to 0.40 mM) were added to Chit/AgNPs (= 10 ml) and Fe^{3+} (= 40 μM). The decay in SPR intensity was monitored at 420 nm with definite time intervals. Figure 5 shows the SPR intensity of AgNPs decreases rapidly with increasing H_2O_2 concentrations, and the orange solution became colorless within ca. 5 min of reaction time. The k_{obs} = 3.1, 4.3, 4.7, 5.4, and 6.5×10^{-3} s^{-1} were calculated from the slopes of log(Absorbance)-time plots for [H_2O_2] = 0.0, 1.0, 2.0, 3.0, and 4.0×10^{-4} mol/L, respectively. The catalytic effect of H_2O_2 might be due to the generation of reactive oxygen species (ROS) during the course of Fenton-like reaction [36]. H_2O_2 is a

Table 1 Effects of Fe^{3+}, pH, and chitosan on the sensing of oxidative dissolution of Chit/AgNPs

[Fe^{3+}] (μM)	[Chit/Ag] (mM)	pH	$10^3 k_{obs}$ (s^{-1})	10^3 kcal (s^{-1})	$(k_{obs} - k_{cal}/k_{obs})$
20	0.8	5.0	3.1	2.9	+0.06
40	0.8	5.0	4.7	5.0	−0.17
60	0.8	5.0	6.7	6.1	+0.08
80	0.8	5.0	7.0	7.0	0.00
100	0.8	5.0	7.6	7.6	0.00
40	0.8	2.0	0.3		
40	0.8	3.5	1.6		
40	0.8	4.5	2.6		
40	0.8	5.5	5.2		
40	0.2	5.0	4.6		
40	0.4	5.0	4.7		
40	0.6	5.0	4.7		
40	1.0	5.0	4.8		

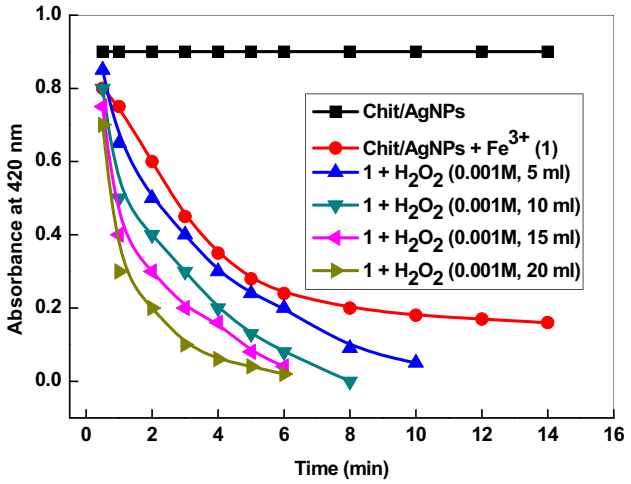

Fig. 5 Effects of H_2O_2 on the SPR intensity decay of AgNPs in the presence of Fe^{3+}. Reaction conditions: [AgNPs] = 8.0×10^{-4} M, [Fe^{3+}] = 20 μM, and pH = 5.0

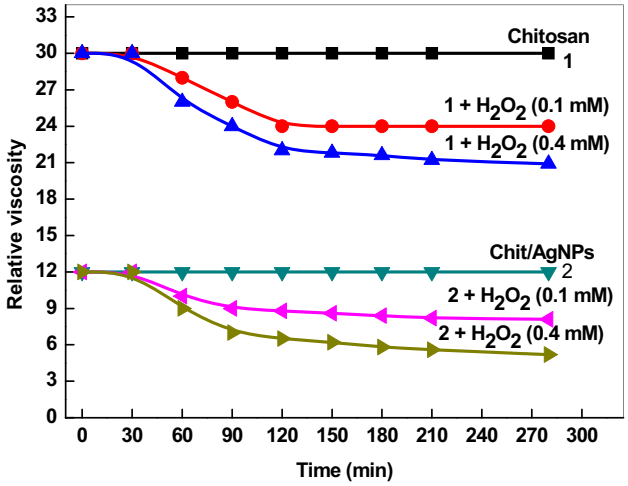

Fig. 6 Plots of relative viscosity versus time for the stability of chitosan and Chit/AgNPs in the presence of H_2O_2

strong oxidizing and reducing agent in acidic and basic reaction media and formed various species (hydroxyl radical, hydroperoxide anion, and superoxide). H_2O_2 reacted with Fe^{3+} ions and generated·OH species ($Fe^{3+} + H_2O_2 \rightarrow Fe^{2+} + HOO^{\cdot} + H^+$; $HOO^{\cdot} + H_2O_2 \rightarrow HO^{\cdot} + O_2^{-\cdot} + H_2O$). The chitosan-$Fe^{3+}$ complex reduced to chitosan-Fe^{2+} in the presence of H_2O_2, and ROS were formed (Eq. 15).

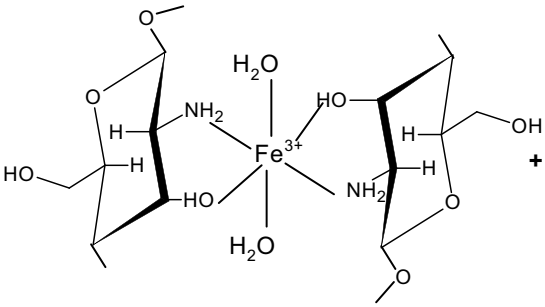

$$\text{+ } H_2O_2 \longrightarrow \textbf{Chitosan-Fe}^{2+}\textbf{ + ROS} \quad (15)$$

Generally, methanol, n-butanol, KI, t-butanol, and benzoquinone are used as scavengers to demonstrate the generation of ROS in Fenton-like reactions [38, 60, 61]. These reagents were used to establish the role of ROS in the oxidation-etching of Chit/AgNPs. Figure S4 (supporting information) shows that the H_2O_2-catalyzed sensing of Fe^{3+} by Chit/AgNPs inhibited in presence of added scavengers. When the quenchers were used as a scavenger for ROS, the rate decreased from 6.5×10^{-3} s^{-1} for H_2O_2 to 4.5, 3.0, 2.8, 2.5, and 2.4×10^{-3} s^{-1} for methanol, n-butanol, KI, benzoquinone (BQ), and t-butanol, respectively. The inhibitory role of scavengers clearly indicates that the $HO^{\cdot}$ and $O_2^{-\cdot}$ were the reactive species and formed as an

The OH is highly reactive and etched the surface of Chit/AgNPs, thus releasing Ag^+ into the reaction solution. Finally, the orange reaction mixture became colorless in the presence of H_2O_2 (Eq. 16).

$$\text{Chit-}(Ag^0)_n + {}^{\cdot}OH + H^+ \longrightarrow \text{Chitosan} + nAg^+ + H_2O \quad (16)$$

(λ_{max} = 420 nm) (Colorless) (16)

intermediate(s) during the Fenton-like reaction between H_2O_2 and Fe^{3+}.

Stability of chitosan and chit/AgNPs in the presence of H_2O_2

Various investigators have used H_2O_2 for the oxidative degradation of chitosan and reported the mechanism of chitosan depolymerization [62, 63]. To gain insight into the interaction of chitosan with H_2O_2, the relative and specific viscosity of aqueous solutions were determined as a function of time with and without H_2O_2 using Eqs. 17 and 18.

$$\eta_{relative} = \frac{\eta_{sample}}{\eta_{solvent}} = \frac{t_{sample}}{t_{solvent}} \tag{17}$$

$$\eta_{specific} = \frac{\eta_{sample} - \eta_{solvent}}{\eta_{solvent}} = \eta_{relative} - 1 \tag{18}$$

where η = viscosity and t = time of out flow. Inspection of Fig. 6 indicates that the chitosan solution (2 ml of 0.2% in sodium acetate buffer of pH 5.0) was stable for ca. 5 h at 30 °C. No change in relative viscosity was observed. Chitosan solution was stable for 30 min in the presence of H_2O_2. At 30 °C, the viscosity decreased by 6.6% and 13.3%, and 16.6% and 20% of the initial value after 1 and 2 h in the presence of 0.1 mM and 0.4 mM H_2O_2, respectively. Chang et al. reported the viscosity of chitosan in 5% acetic acid decreased 82% from the initial value after the treatment of chitosan solution with 3.5% H_2O_2 for 15 min at 80 °C [64]. The viscosity of Chit/AgNPs (= 10.0×10^{-4} mol/L) was also decreased with time in the presence of H_2O_2. The decrease in viscosity might be due to the hydrolysis of the glycoside chain of chitosan with ROS generated via Fenton-type reaction.

The present system became more complicated after the addition of H_2O_2 in Chit/AgNPs + Fe^{3+} solution (Scheme 2).

Scheme 2 represents the three reactions of oxidative dissolution of AgNPs, cleavage of glycosidic linkage, and generation of ROS by the interaction of the Chit/AgNP–Fe^{3+} redox system with H_2O_2. Out of these, the Fenton reaction between Fe^{3+} + H_2O_2 was very fast [37]. The oxidative dissolution of CTAB-capped AgNPs with BH_4^- and H_2O_2 was slow; $k_{obs} = 2.0 \times 10^{-6}$ and 5.2×10^{-4} s^{-1}, respectively [43]. Chitosan was stable with H_2O_2 for ca. 1 h (Fig. 6). The reaction of AgNPs and Fe^{3+} was complete within ca. 10 min of reaction time (Fig. 2). Thus, we may safely conclude that the added H_2O_2 reacted with Fe^{3+} and generated ROS, which reacted with Chit/AgNPs, and the orange color completely dissolved very rapidly. Chit/AgNPs are an excellent nanosensor for H_2O_2 and Fe^{3+} [27, 35–40].

Optical sensing for metal ions

In order to determine the selectivity of the sensor, the optimal concentration of Chit/AgNPs (1.0 mM) was added separately in a series of conical flasks containing the same concentration (0.10 mM) of different metal ions, i.e. Na^+, K^+, Ba^{2+}, Ca^{2+}, Cu^{2+}, Co^{2+}, Mg^{2+}, Ni^{2+}, Pb^{2+}, Zn^{2+}, Al^{3+}, and Fe^{3+}. The UV–visible spectrum of each metal ion solution was recorded after 20 min of mixing of AgNPs under the same condition. Figure S5 (supporting information) showed a slight change in the SPR intensity of AgNPs, and the added ions had no effect on the position of the SPR band (remained constant for all metal ions). For Fe^{3+}, the SPR intensity reduced completely, and the orange solution changed to colorless, indicating the high sensitivity of Chit/AgNPs toward Fe^{3+} ions (Fig. 7). The change in SPR intensity was also plotted against each metal ion, and results are presented in Fig. 7, which demonstrates that the added metal ion has no significant effect on the absorbance of AgNPs. Optical images also show that the orange color became colorless after the mixing of Fe^{3+} ions into AgNPs solution within 20 min. The effect of other metal ions was further investigated by mixing an equimolar solution of Fe^{3+} ions and other metal ions. The color change was monitored under similar experimental procedure used for Fe^{3+}. We did not observe significant interference of added foreign ions. Chit/AgNPs are an

Scheme 2 Possible interaction of H_2O_2 with chitosan, AgNPs, and Fe^{3+}

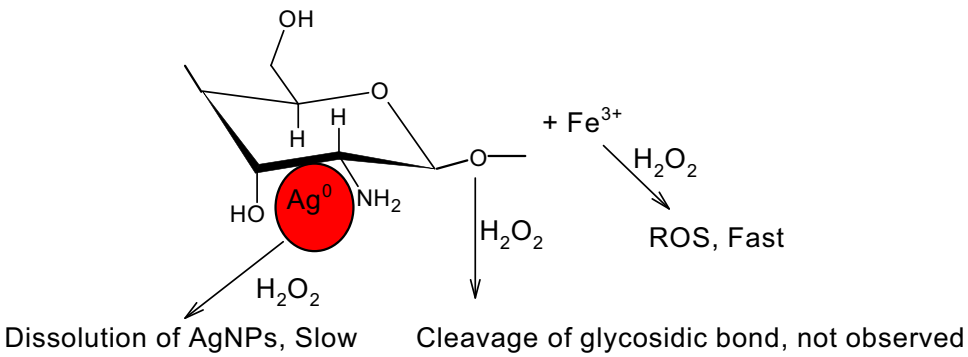

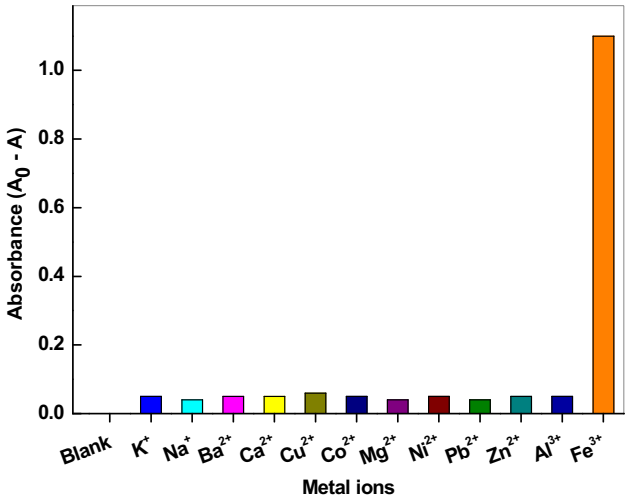

Fig. 7 Sensor response for detecting Fe^{3+} ions with different metal ions. Reaction conditions: [AgNPs] = 10.0×10^{-4} M, [metal ions] = 1.0×10^{-4} M, and pH = 5.0

excellent selective sensor for Fe^{3+} ions. The % error was estimated with the formula [($A_0 - A$ of Fe^{3+} $- A_0 - A$ with coexisting ions/$A_0 - A$ of Fe^{3+}) × 100]. Table 2 shows that the interference of foreign ions was lowest under the experimental conditions.

Antimicrobial activity of chitosan and Chit/AgNPs

Chitosan has large number of $–NH_2$ and –OH groups and is soluble in acidic media due to the protonation of glucosamine units ($–NH_2$ group) into soluble form ($–NH_3^+$). Its solubility depends on the degree of acetylation, molecular weight, and type of chitosan biological origin. It has strong binding capacity with any possible free metal ions and a negatively charged microbial cell protein membrane via electrostatic interactions. The growth inhibition kinetic method was used to evaluate the antibacterial activity of chitosan and Chit/AgNPs against Gram-positive and Gram-negative human pathogens. The control experiments were performed with standard gentamicin for antibacterial

Table 2 Effect of interfering metal ion concentration (= 1.0×10^{-4} M) on the estimation of Fe^{3+} = 1.0×10^{-4} M

Interfering ion	Error (%)	Interfering ion	Error (%)
Na^+	3.6	Mg^{2+}	3.6
K^+	4.1	Ni^{2+}	4.1
Ba^{2+}	3.6	Pb^{2+}	3.6
Ca^{2+}	4.2	Al^{3+}	3.5
Co^{2+}	4.3	Zn^{2+}	5.4
Cu^{2+}	5.4		

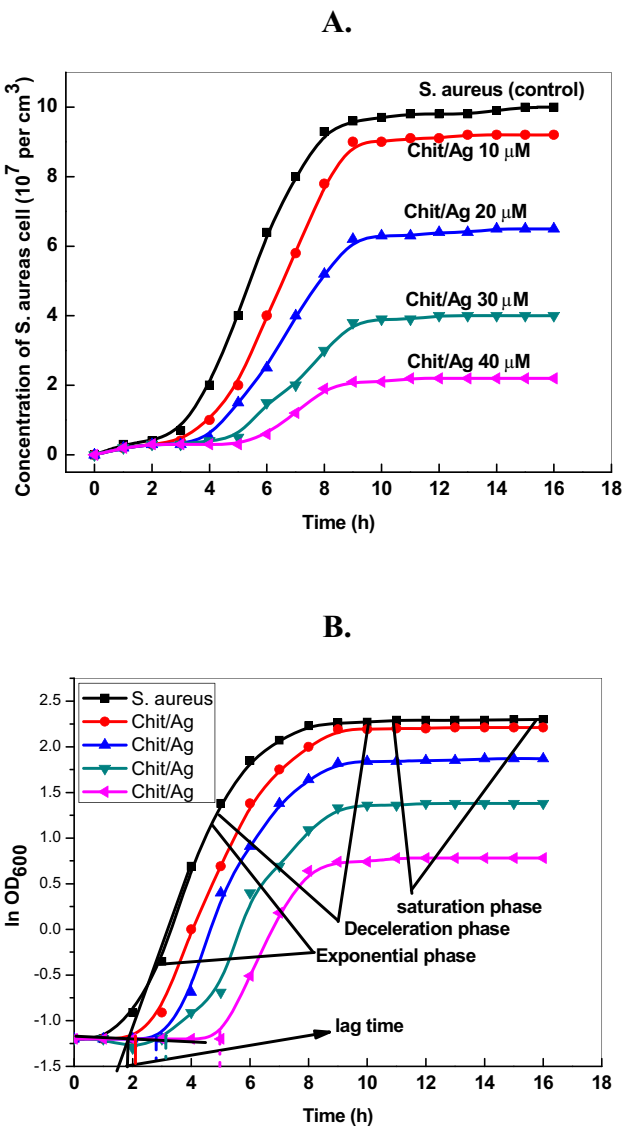

Fig. 8 Typical bacterial kinetic growth plots [cell concentration versus time (**A**) and ln OD versus time (**B**)] for *S. aureus* growth with Chit/AgNPs and chitosan

activity. The antimicrobial efficiency was also estimated by calculating the zone of inhibition using a previously reported method [65]. The diameter of each inhibition zone was measured in millimeters and was found to be 10, 18, 25, and 32 mm for *S. aureus* and 15, 20, 26, and 35 mm for *E. coli* against varying concentrations of Chit/AgNPs. Figure 8A shows the growth kinetics of chitosan and Chit/AgNPs by optical density measurements at 600 nm. It can be observed that the Chit/AgNPs are more potent than pure chitosan or $AgNO_3$. The growth rate constants were evaluated from the slopes of Fig. 8B and were found to be 4.1, 3.8, 3.3, and 2.6×10^{-3} min^{-1} for 10, 20, 30, and 40 μM of Chit/AgNPs, respectively. The mechanism of antimicrobial activity of chitosan and Chit/AgNPs against

human pathogens might be due to electrostatic interactions between the $–NH_3^+$ and the bacterial cell wall negative residues. The surfaces of human pathogens have a negative charge. The coordinated and/or adsorbed chitosan prevents the transport of essential nutrients (sodium, potassium, and calcium ions) into the bacterial cell membrane, which disturbs the osmotic imbalance. As a result, chitosan kills or hampers the growth of bacteria. Chitosan has been found to act as a bactericidal and bacteriostatic agent against human pathogens [66]. On the other hand, AgNPs coordinated with protein and also disturbed the function of the bacteria cell wall. Chit/AgNPs exhibited higher microbial activity than that of pure chitosan or AgNPs, which might be due to the synergistic effects of the combination of chitosan and AgNPs (Scheme 3).

Chi-AgNPs were incorporated into the bacterial cell wall. Anionic residue of protein amino acid (especially cysteine) coordinated with the positive surface of AgNPs, which underwent one-electron transfer (oxidation–reduction) from the thiol moiety of cysteine to the AgNPs via molecular oxygen. As a result, Ag^+ was released into the bacterial cell and coordinated with the –carboxylate (COO^- group). It is well known that the toxicity of AgNPs depends on the concentration, composition, size, shape, surface charge, surface functionalization, solubility, and release of silver ions [67]. Kittler et al. reported that the toxicity of AgNPs depends on the rate and degree of dissolution of AgNPs (release of silver ions) [68]. The aged AgNPs were more toxic to cells than freshly synthesized AgNPs. Thus, we may confidently state that Ag^+ ions are released by the surface oxidation of AgNPs under physiological conditions in vivo, which can influence the antimicrobial activity of the AgNPs [69].

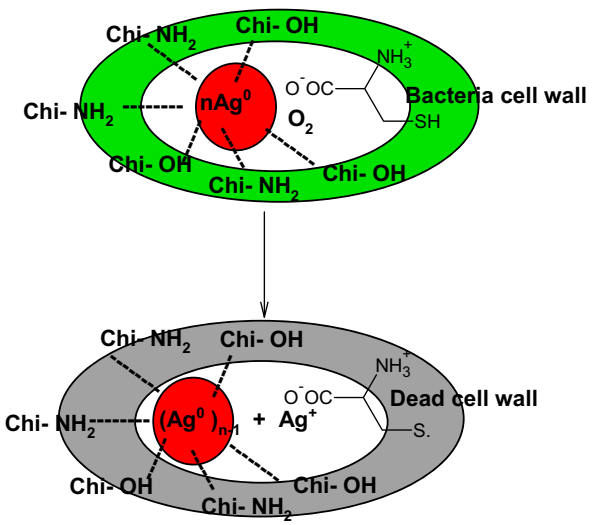

Scheme 3 Mechanism action of Chi-AgNPs with the bacteria cell wall

Conclusion

We demonstrated a simple method for the fabrication of chitosan-capped AgNPs. UV–visible absorption and TEM characterization showed that the AgNPs were polydisperse and spherical, with average diameter of 12.5 nm and a strong SPR band at 420 nm. Chit/AgNPs were used as a sensor for the detection of Fe^{3+} in aqueous media, exhibiting excellent sensitivity and selectivity. An oxidation–reduction mechanism was proposed for the dissolution of AgNPs by Fe^{3+}. Chitosan acted as a coordinating agent, which formed a complex with Fe^{3+} and inhibited dissolution. The specific viscosity of chitosan and Chit/Ag remained unchanged for 1 h in the presence of H_2O_2 from 0.1 mM to 0.4 mM at 30 °C. The dissolution rates accelerated with increasing H_2O_2 concentration at a fixed amount of Fe^{3+}. The rates of Chit/AgNP-assisted growth of bacteria were higher than those with pure chitosan. Adsorption of chitosan on the surface of the cell wall prevented the transport of essential electrolytes due to the bactericidal and bacteriostatic properties of chitosan. These results suggest that the chitosan polymer chain was stable with a small concentration of H_2O_2 at pH ca. 5.0 and exerted no interference in the sensing of AgNPs for the detection of Fe^{3+}.

Supplementary information The online version contains supplementary material available at https://doi.org/10.1007/s10965-021-02673-0.

Acknowledgements This project was funded by the Deanship of Scientific Research (DSR) at King Abdulaziz University, Jeddah, under grant no. G:93-247-1441. The author, therefore, acknowledges with thanks DSR for technical and financial support.

References

1. Mahal A, Khullar P, Kumar H, Kaur G, Singh N, Jelokhani-Niaraki M, Bakshi MS (2013) ACS Sustain Chem Eng 1:627–639
2. Reicha FM, Sarhan A, Abdel-Hamid MI, El-Sherbiny IM (2012) Carbohydr Polym 89:236–244
3. Zhang J-J, Gu M-M, Zheng T-T, Zhu J-J (2009) Anal Chem 81:6641–6648
4. Mohan YM, Raju KM, Sambasivudu K, Singh S, Sreedhar B (2007) J Appl Polym Sci 106:3375–3381
5. Shervani Z, Yamamoto Y (2011) Carbohydr Res 346:651–658
6. Hong KH, Park JL, Sul IH, Youk JH, Kang TJ (2006) J Polym Sci Part B Polym Phys 44:2468–2474
7. Rong H, Xuefeng Q, Jie Y, Zikang Z (2002) J Mater Chem 12:3783–3786
8. Iqbal S, Zahoor C, Musaddiq S, Hussain M, Begum R, Irfan A, Azam M, Farooqi ZH (2020) Ecotoxicol Environ Saf 202:110924
9. Hussain I, Farooqi ZH, Ali F, Begum R, Irfan A, Wu W, Wang X, Shahid M, Nisar J (2021) J Mol Liq 335:116106
10. Khan Z (2019) Int J Biol Macromol 136:165–176
11. Bakshi MS, Possmayer F, Petersen NO (2007) J Phys Chem C 111:14113–14124
12. Salem MA, Bakr EA, El-Attar HG (2018) Spectrochimica Acta Part A 188:155–163

13. Shen C, Shen Y, Wena Y, Wang H, Liu W (2011) Water Res 45:5200–5210
14. Zimmermann AC, Mecabo A, Fagundes T, Rodrigues CA (2010) J Hazard Mater 179:192–196
15. Rashid S, Shen C, Chen X, Li S, Chen Y, Wen Y, Liu J (2015) RSC Adv 5:90731–90741
16. Begum R, Najeeb J, Ahmad G, Wu W, Irfan A, Al-sehemi AG, Farooqi ZH (2018) React Funct Polym 132:89–97
17. Begum R, Farooqi ZH, Aboo AH, Ahmed E, Sharif A, Xiao J (2019) J Hazard Mater 377:399–408
18. Begum R, Ahmad G, Najeeb J, Wu W, Irfan A, Azam M, Nisar J, Farooqi ZH (2021) Chem Phys Letters 763:138263
19. Farooqi ZH, Sultana H, Begum R, Usman M, Ajmal M, Nisar J, Irfan A, Azam M (2020) Int J Environ Anal Chem. https://doi.org/10.1080/03067319.2020.1779247
20. El-Sherbiny IM, Hefnawy A, Salih E (2016) Int J Biol Macromol 86:782–788
21. Sugunan A, Thanachayanont C, Dutta J, Hilborn JG (2005) Sci Technolo Adv Mater 6:335–340
22. Sharma P, Mourya M, Choudhary D, Goswami M, Kundu I, Dobhal MP, Tripathi CSP, Guin D (2018) Sens Actuators B Chem 268:310–318
23. Jiang H, Chen Z, Cao H, Huang Y (2012) Analyst 137:5560–5564
24. Yoosaf K, Ipe BI, Suresh CH, Thomas KG (2007) J Phys Chem C 111:12839–12847
25. Chen Z, Zhang X, Cao H, Huang Y (2013) Analyst 138:2343–2349
26. Ou K-L, Hsu T-C, Liu Y-C, Yang K-H, Sun W-H (2013) J Electroanal Chem 702:66–71
27. Gao X, Lu Y, He S, Li X, Chen W (2015) Anal Chim Acta 879:118–125
28. Duan J, Yin H, Wei R, Wang W (2014) Biosens Bioelectron 57:139–142
29. Annadhasan M, Muthukumarasamyvel T, Babu VRS, Rajendiran N (2014) ACS Sustain Chem Eng 2:887–896
30. Zhou Y, Zhao H, Li C, He P, Peng W, Yuan L, Zeng L, He Y (2012) Talanta 97:331–335
31. Naseem K, Farooqi ZH, Begum R, Ghufran M, Rehman MZ, Najeeb J, Irfan A, Al-Sehemi AG (2018) J Mol Liq 268:229–238
32. Naseem K, Begum R, Wu W, Usman M, Irfan A, Al-Sehemi AG, Farooqi ZH (2019) J Mol Liq 277:522–531
33. Naseem K, Begum R, Farooqi ZH, Wu W, Irfan A (2020) Appl Organomet Chem 34:e5742
34. Hernandez RB, Franco AP, Yola OR, Lopez-Delgado A, Felcman J, Recio MAL, Merce ALR (2008) J Mole Structu 877:89–99
35. Cobley CM, Rycenga M, Zhou F, Li Z-Y, Xia Y (2009) J Phys Chem C 113:16975–16982
36. Guo X, Zhang Q, Sun Y, Zhao Q, Yang J (2012) ACS Nano 6:1165–1175
37. Garrido-Ramíreza EG, Theng BKG, Mora ML (2010) Applied Clay Sci 47:182–192
38. Wang G-L, Zhu X-Y, Dong Y-M, Jiao H-J, Wu X-M, Li Z-J (2013) Talanta 107:146–153
39. Vasileva P, Donkova B, Karadjova I, Dushkin C (2011) Colloids Surfaces A: Physicochem Eng Aspects 382:203–210
40. Wang H, Wang H, Li T, Ma J, Li K, Zuo X (2017) Sens Actuators B Chem 239:1205–1212
41. Tagad CK, Dugasani SR, Aiyer R, Park S, Kulkarni A, Sabharwal S (2013) Sens Actuators B Chem 183:144–149
42. Mohan S, Oluwafemi OS, George SC, Jayachandran VP, Lewu FB, Songca SP, Kalarikkal N, Thomas S (2014) Carbohydr Polym 106:469–474
43. Albeladi AB, AL-Thabaiti SA, Khan Z (2020) J Mol Liq 302:112565
44. Tsao CT, Chang CH, Lin YY, Wu MF, Han JL, Hsieh KH (2011) Carbohyd Res 346:94–102
45. Roberts GAF, Domszy JG (1982) Int J Biol Macromol 4:374–377
46. Sondi I, Salopek-Sondi B (2004) J Colloid Interface Sci 275:177–182
47. Mie G (1908) Ann Phys 25:377–455
48. Sun Y, Xia Y (2003) Analyst 128:686–691
49. Link S, El-Sayed MA (1999) J Phys Chem B 103:8410–8426
50. Deivaraj TC, Lala NL, Lee JY (2005) J Colloid Interface Sci 289:402–409
51. Al-Ghamdi AD, Zaheer Z, Aazam ES (2020) Saudi Pharmaceutical J 28:1035–1048
52. Shankar SS, Rai A, Ahmad A, Sastry M (2004) J Colloid Interf Sci 275:496–502
53. Khullar P, Singh V, Mahal A, Dave PN, Thakur S, Kaur G, Singh J, Kamboj SS, Bakshi MS (2012) J Phys Chem C 116:8834–8843
54. Ali SW, Rajendran S, Joshi M (2011) Carbohyd Polym 83:438–446
55. Kabir-ud-Din, Salem JKJ, Kumar S, Rafiquee MZA, Khan Z (1999) J Colloid Interface Sci 213:20–28
56. Kabir-ud-Din, Rafiquee MZA, Akram M, Khan Z (1999) Int J Chem Kinet 31:103–111
57. Cotton FA, Wilkinson G (1980) Advanced Inorganic Chemistry-A Comprehensive Text, 4th ed. Wiley, p 758
58. Henglein A (1993) J Phys Chem 97:5457–5471
59. Goia DV, Matijevic E (1998) New J Chem 1203–1215
60. Devi LG, Kumar SG, Reddy KM, Munikrishnappa C (2009) J Hazard Mater 164:459–467
61. Khan Z, Al-Thabaiti SA (2018) J Photochem Photobiolo B: Biology 180:259–267
62. Qin CQ, Du YM, Xiao L (2002) Polym Degrad Stab 76:211–218
63. Tian F, Liu Y, Hu K, Zhao B (2003) J Mater Sci 38:4709–4712
64. Chang KLB, Tai M-C, Cheng F-H (2001) J Agric Food Chem 49:4845–4851
65. Kadam D, Momin B, Palamthodi S, Lele SS (2019) Carbohydr Polym 211:124–132
66. Roller S, Covill N (1999) Int J Food Microbiolo 47:67–77
67. Beera C, Foldbjerga R, Hayashib Y, Sutherlandb DS, Autrupa H (2012) Toxicol Lett 208:286–292
68. Kittler S, Greulich C, Diendorf J, Kcoller M, Epple M (2010) Chem Mater 22:4548–4554
69. Lok CN, Ho CM, Chen R, He QY, Yu WY, Sun H, Tam PK, Chiu JF, Che CM (2007) J Biol Inorg Chem 12:527–534